THE ANNALS OF "DUNAREA DE JOS" UNIVERSITY OF GALATI
FASCICLE IX. METALLURGY AND MATERIALS SCIENCE
N°. 4 - 2024, ISSN 2668-4748; e-ISSN 2668-4756
Article DOI: https://doi.org/10.35219/mms.2024.4.06

ENHANCED RETINAL VESSEL DETECTION USING GRADIENT PYRAMID FUSION ALGORITHM

Cristian-Dragoș OBREJA
Department of Materials and Environmental Engineering, Faculty of Engineering, "Dunarea de Jos" University of Galati 47 Domneasca, 800008 Galati, Romania
e-mail: cristian.obreja@ugal.ro

ABSTRACT

The main goal of this study is to create an innovative approach to retinal vessel detection using the gradient pyramid fusion algorithm to improve edge continuity and measurement precision in retinal images. Traditional methods, like wavelet transform and guided filter, face challenges with background noise, artifacts and uneven illumination, which can distort vessel measurement. The proposed fusion method manages to overcome these limitations by combining the strengths of traditional techniques, which creates more continuous edges through gradient fusion across multiple scales, thus managing to also limit the number of image artifacts. We used images from the DRIVE database, to evaluate the fusion algorithm's precision, with results showing improved vascular tree detection and continuous edges, a reduction in the number of artifacts and improved measurement accuracy. The results show that this image fusion method improves the retinal image analysis, thus helping in early disease diagnosis.

KEYWORDS: wavelet transform, gradient pyramid fusion, edge detection, image fusion, guided filter

1. Introduction

Retinal image analysis is playing an important role in early detection and diagnosis of ocular and systemic diseases, especially those concerning the vascular system, such as diabetic retinopathy and hypertension. Vascular abnormalities, such as those generated by diabetic retinopathy, often require accurate measurement, however, asymmetry in vessels and complex backgrounds are usually some of the motives contributing to the lack of precision in vessel diameter measurements [1-3]. Most algorithms today detect blood vessels using techniques related to segmentation, probing or edge detection. These are realized by using various gradient masks for edge detection. Furthermore, morphological operations are carried out to obtain accurate edge maps especially for noise affected images. Thresholding is a fundamental method of image segmentation, which separates foreground (in our case, blood vessels) from background [4-9]. Moreover, advanced threshold techniques continue to enhance information coming from localized areas of an image. Probing methodology uses algorithms in which a vessel path is tracked while detecting edges in a real time manner. However, these bear serious limitations due to background noise and uneven illumination, thereby making quantitative measurements difficult [10-14]. In this paper the gradient pyramid image fusion algorithm represents a new method used to overcome such limitations by merging the merits of different traditional filters. [10] Using a merged representation of gradient pyramids, the technique proposed here attempts to generate sharper and more continuous edges without affecting any important useful information in the retinal images. The performance of the GPF algorithm for producing high-quality vascular edge maps and accurate measurement values of retinal vessel diameter is assessed in this paper. [14-16]

The structure of the paper is organised in four sections, the firs one is introduction. Section 2 covers materials and methods, while Sections 3 present experimental results and discussion. Conclusions are provided in Section 5.

2. Materials and methods

2.1. Database and the Algorithm

A total of 40 retinal images from the DRIVE digital retinal image database were analysed [17].

THE ANNALS OF "DUNAREA DE JOS" UNIVERSITY OF GALATI
FASCICLE IX. METALLURGY AND MATERIALS SCIENCE
N°. 4 - 2024, ISSN 2668-4748; e-ISSN 2668-4756
Article DOI: https://doi.org/10.35219/mms.2024.4.06

This dataset consists of 20 randomly selected images and 20 manually segmented images, which serve as ground truth. Figure 1 illustrates the flowchart of the proposed method.

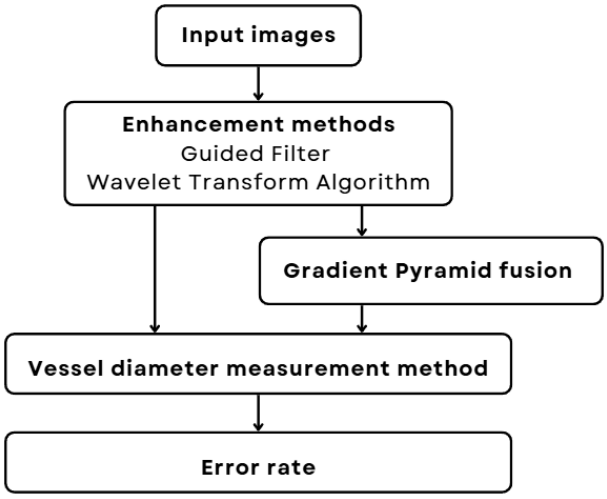

Fig. 1. *Flow chart of the proposed method*

2.2. Guided Filter (GF)

It is an image processing technique that has wide applications in edge-preserving, smoothing, noise reduction, and detail enhancement. It differs from other basic averaging filters, which blur edges across the board, in that it smooths out with the preservation of edges. The main steps of the guided filter are: computation of the mean and variance of the guidance image, calculate the correlation between the guidance image and the input image, use these values in generating filtering coefficients and apply these coefficients to produce the final filtered image. The algorithm is based on a set of equations [18-20]. Local means of the input image and guidance image are computed using a window of size determined by the radius:

$$\mu_G = \frac{1}{|\omega|}\sum_{i\epsilon\omega} G(i), \mu_I = \frac{1}{|\omega|}\sum_{i\epsilon\omega} I(i)$$

where ω *is the* number of pixels in the local window.

In the next step, we calculate the variance of the guidance image locally, covariance between the guidance and the input image as:

$$\sigma_G^2 = \frac{1}{|\omega|}\sum_{i\epsilon\omega}(G(i) - \mu_G)^2$$

$$\sigma_{IG} = \frac{1}{|\omega|}\sum_{i\epsilon\omega}(G(i) - \mu_G)(I(i) - \mu_I)$$

The filtering coefficients a and b are then calculated, with the former controlling the detail adaptation rate:

$$a = \frac{\sigma_{IG}}{\sigma_G^2 + \varepsilon}$$

$$b = \mu_I - a * \mu_G$$

where ε represents the regularization constant to control the edge preservation level. Furthermore, the final filtered image is obtained by the local weighted average of coefficients:

$$Q(i) = a * G(i) + b$$

This filter finds frequent application in image denoising and detail amplification because of the great efficiency and versatility in maintaining important structural features of images [18].

2.3. Wavelet Transform-Based Algorithm (WT)

The Wavelet Transform-Based Enhancement algorithm is a sophisticated method in image processing aimed at reducing noise and bringing out finer details. It works by breaking down an image into frequency components through the Discrete

THE ANNALS OF "DUNAREA DE JOS" UNIVERSITY OF GALATI
FASCICLE IX. METALLURGY AND MATERIALS SCIENCE
N°. 4 - 2024, ISSN 2668-4748; e-ISSN 2668-4756
Article DOI: https://doi.org/10.35219/mms.2024.4.06

Wavelet Transform (DWT). This decomposition allows the separation of low-frequency components (representing the main structure of the image) from high-frequency components (containing fine details and noise). By adjusting each component selectively, this approach balances noise reduction with detail enhancement [21].

The algorithm involves four primary stages: wavelet decomposition, noise reduction, detail enhancement, and wavelet reconstruction, each governed by specific mathematical operations:

• Wavelet Decomposition: The image is split into multiple levels, yielding a vector of wavelet coefficients (C) and a structure (S) that defines each level's size. This is represented by the equation:

$$C, S = wavedec2(I, decomposition\_level, wavelet\_type)$$

• Noise Reduction: Using a technique called soft thresholding, noise is reduced by setting small, noisy details to zero, preserving significant parts. This operation is expressed as:

$$\mathrm{d}\_thresholded = sign(d) \cdot max(|\, d\,| - noise\_threshold, 0)$$

• Detail Enhancement: Here, the remaining details are boosted by multiplying specific wavelet coefficients by a "detail factor," enhancing edges and finer structures. This is shown with:

$$d\_enhanced = \mathrm{d}\_thresholded \cdot detail\_factor$$

• Wavelet Reconstruction: Finally, all modified coefficients are combined to reconstruct an enhanced image using the inverse wavelet transform:

$$I\_enhanced = waverec2(C\_modified\ , S, wavelet\_type).$$

This method improves image quality by reducing unwanted noise and emphasizing edges, yielding a cleaner, sharper result [22].

2.4. Gradient Pyramid fusion algorithm (GPF)

The Gradient Pyramid fusion algorithm combines multiple images by capturing and merging key details across varying scales. It starts by decomposing each input image into a pyramid of gradient images, which represents intensity changes at multiple scales. Each pyramid level highlights gradients that reveal shifts in intensity, isolating critical features in each image.

The algorithm then proceeds with the fusion stage, where it creates gradient pyramids for each input image and selects the maximum gradient at every level. This selection effectively merges the most prominent details from both images into a unified gradient pyramid. The fused pyramid is then used to reconstruct a single, cohesive image that retains essential details from the original inputs.

The process involves several key steps: constructing the gradient pyramid by calculating gradient magnitudes using Sobel filters, down sampling each level with pyramid (using 'reduce') for each RGB channel, and expanding each pyramid level in the reconstruction stage to add it to the level below. This process is repeated independently for each colour channel to produce a final, full-colour RGB image. Finally, the algorithm saves and displays the original images, the gradient pyramids, and the fused image, providing a clear view of how features from the input images combine into a refined, enhanced result [23-25].

At each level l in the pyramid, the fused gradient $G_F^{(l)}$ is obtained by selecting the maximum gradient values from each pixel of the two input images, $G_A^{(l)}$ and $G_B^{(l)}$:

$$G_F^{(l)}(x,y) = \max(G_A^{(l)}(x,y), G_B^{(l)}(x,y))$$

where $G_A^{(l)}$ is the gradient of image A at level l, $G_B^{(l)}$ is the gradient of image B at level l, $G_F^{(l)}$ is the fused gradient at level l and (x,y) are the pixel coordinates. This equation selects the strongest edges at each level and pixel position, ensuring that the most prominent features from both images are preserved.

THE ANNALS OF "DUNAREA DE JOS" UNIVERSITY OF GALATI
FASCICLE IX. METALLURGY AND MATERIALS SCIENCE
Nº. 4 - 2024, ISSN 2668-4748; e-ISSN 2668-4756
Article DOI: https://doi.org/10.35219/mms.2024.4.06

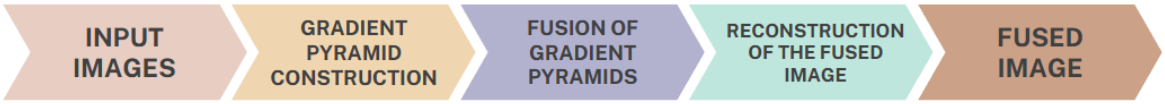

Fig. 2. *Flow chart of the fusion algorithm*

2.5. Vessel Diameter Measurement

The vessel diameter measurement method outlined here uses a series of precise image processing steps to accurately detect and analyse vessel diameters. It begins with contrast enhancement through CLAHE (Contrast Limited Adaptive Histogram Equalization), which boosts vessel visibility by enhancing contrast [26]. Next, edge detection via the Canny method identifies vessel boundaries, with an optional morphological closing step to seal small gaps in these edges.

Afterward, skeletonization reduces the vessel image to a single-pixel-wide structure, simplifying the geometry for measurement. A distance transform then calculates the Euclidean distance from each pixel to the nearest edge; doubling this distance gives an estimated diameter at each skeleton point. Finally, all non-zero diameter values are collected, and the mean diameter is calculated and presented for analysis [27].

Fig. 3. *Flow chart of the vessel diameter measurement algorithm*

3. Results and discussion

To evaluate the proposed fusion algorithm's performance relative to traditional filters, tests were conducted on a set of 20 randomly selected retinal images. Figure 4 provides examples of vascular maps generated using the Gradient Pyramid fusion, Wavelet Transform-based algorithm, and Guided Filter. Diameter measurements were made for retinal vessels across all images, comparing processed, fused, and ground truth data for a comprehensive assessment.

Fig. 4. *Examples of vascular map. (a) Original input image; (b) ground truth image; (c) Guided filter; (d) Wavelet transform-based filter; (e) Gradient Pyramid fusion*

Figure 5 shows examples of vascular maps produced during the different stages of the vessel diameter measurement algorithm. The processed images (both by guided filter and wavelet algorithm) together with the fused image, are used as input information for the vessel diameter measurement algorithm. Over this images a contrast enhancement algorithm is applied, followed by Canny edge detector. Finally, a skeletonization operation is made and the blood vessel diameter map is generated, followed by the diameter's values measurement.

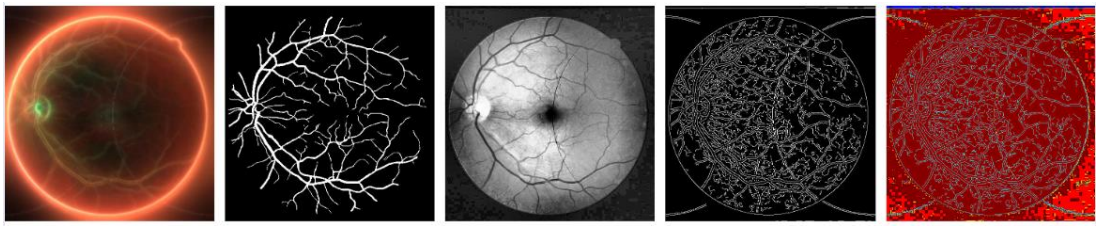

Fig. 5. *Examples of vascular map. (a) Fused image; (b) ground truth image; (c) CLAHE filter; (d) Canny edge detection; (e) Blood vessel diameter map*

THE ANNALS OF "DUNAREA DE JOS" UNIVERSITY OF GALATI
FASCICLE IX. METALLURGY AND MATERIALS SCIENCE
Nº. 4 - 2024, ISSN 2668-4748; e-ISSN 2668-4756
Article DOI: https://doi.org/10.35219/mms.2024.4.06

Table 1 displays the average vessel diameter values along with the associated error rates for the Gradient Pyramid fusion, Wavelet Transform-based algorithm, and Guided Filter.

This paper examines the Gradient Pyramid fusion algorithm's ability to generate highly accurate edge maps, particularly for measuring retinal vessel diameters and calculating error rates. One major advantage of this fusion method is its capability to produce uninterrupted edges.

Table 1. *The average vessel diameter values and the average percentage error*

Ground truth	GF	e_{GF}%	WT	e_{WT}%	GPF	e_{GPF}%
2.210	2.097	5.128	2.098	5.053	2.137	3.318

As shown in Table 1, the average vessel diameters and error percentages are reported for manually segmented, filtered, and fused retinal images. Among traditional filters, the wavelet transform-based filter (WT) shows the lowest error rates. WS's average error rate is 5.053%, while GF's error rate is 5.053%. The GPF fusion further improves accuracy, with an error rate of 3.318%.

As illustrated in Figure 4, the WT and GF filters enhance the image and improve edges, but there are still areas where there is not enough of a difference between the blood vessel edge and the background. Furthermore, the fusion method achieves greater accuracy and lower error rates than traditional filters. Gradient Pyramid fusion yields the highest alignment with the ideal edge map, as defined by manual segmentation. Traditional enhancement algorithms may lack precision, while the fusion technique effectively combines the strengths of both filters to achieve smooth, continuous edges without over-detection.

Despite the additional edges from distorted vessels in retinopathy maps, GPF fusion consistently outperforms conventional filters in identifying true edges. By merging the outputs of WT and GF, this fusion method enhances the accuracy of retinal images more effectively than either filter alone.

4. Conclusions

This study demonstrates the Gradient Pyramid Fusion (GPF) algorithm's effectiveness in producing accurate, high-quality edge maps for retinal images, particularly for vessel diameter measurement. By combining the strengths of the Wavelet Transform (WT) and Guided Filter (GF), GPF significantly improves accuracy, continuity, and edge definition over traditional filters. Supported by quantitative analysis, the results show that GPF excels at preserving essential structural features while reducing error rates, making it a promising tool for advancing retinal image analysis and other applications that demand precise edge detection and image enhancement.

References

[1]. Abràmoff M. D., Lavin P. T., Birch M., Shah N., Folk J. C., *Pivotal trial of an autonomous AI-based diagnostic system for detection of diabetic retinopathy in primary care offices*, Digital Medicine, 1(1), p. 1-8, https://doi.org/10.1038/s41746-018-0040-6, 2018.

[2]. Antal B, Hajdu A., *An ensemble-based system for microaneurysm detection and diabetic retinopathy grading*, IEEE Transactions on Bio-medical Engineering, 59(6), p. 1720-1726, DOI: 10.1109/tbme.2012.2193126, 2012.

[3]. Fraz M. M., *et al.*, *Blood vessel segmentation methodologies in retinal images–a survey*, Computer Methods and Programs in Biomedicine, 108 (1), p. 407-433, https://doi.org/10.1016/j.cmpb.2012.03.009, 2012.

[4]. Niemeijer M., *et al.*, *Retinopathy online challenge: automatic detection of microaneurysms in digital color fundus photographs*, IEEE Trans Med Imaging, 29(1), p. 185-95, doi: 10.1109/TMI.2009.2033909, 2010.

[5]. Staal J., *et al.*, *Ridge-based vessel segmentation in color images of the retina*, IEEE Transactions on Medical Imaging, 23 (4), p. 501-509, https://doi.org/10.1109/TMI.2004.825627, 2004.

[6]. Zana F., Klein J. C., *Segmentation of vessel-like patterns using mathematical morphology and curvature evaluation*, IEEE Transactions on Image Processing, 10 (7), p. 1010-1019, https://doi.org/10.1109/83.931095, 2001.

[7]. Hoover A., Kouznetsova V., Goldbaum M., *Locating blood vessels in retinal images by piecewise threshold probing of a matched filter response*, IEEE Transactions on Medical Imaging, 19 (3), p. 203-210, https://doi.org/10.1109/42.845178, 2000.

[8]. Soares J. V., *et al.*, *Retinal vessel segmentation using the 2-D Gabor wavelet and supervised classification*, IEEE Transactions on Medical Imaging, 25 (9), p. 1214-1222, https://doi.org/10.1109/TMI.2006.879967, 2006.

[9]. Yin Y., Adel M., Bourennane S., *Retinal vessel segmentation using a probabilistic tracking method*, Pattern Recognition, 45 (4), p. 1235-1244, https://doi.org/10.1016/j.patcog.2011.09.019, 2012.

[10]. Kaur H., Koundal D., Kadyan V., *Image Fusion Techniques: A Survey*, Arch Computat Methods Eng, 28, p. 4425-4447, https://doi.org/10.1007/s11831-021-09540-7, 2021.

[11]. Budai A., *et al.*, *Robust vessel segmentation in fundus images*, International Journal of Biomedical Imaging, Article 154860, https://doi.org/10.1155/2013/154860, 2013.

[12]. Al-Diri B., Hunter A., Steel D., *An active contour model for segmenting and measuring retinal vessels*, IEEE Trans Med Imaging, 28(9), p. 1488-97, doi: 10.1109/TMI.2009.2017941, 2009.

[13]. Zhang B., *et al.*, *Retinal vessel extraction by matched filter with first-order derivative of Gaussian*, Computer Methods and Programs in Biomedicine, 122 (3), p. 168-179. https://doi.org/10.1016/j.cmpb.2015.08.008, 2015.

[14]. Dashtbozorg B., *et al.*, *An automatic graph-based approach for artery/vein classification in retinal images*, IEEE Trans Image Process, 23(3), p. 1073-83, doi: 10.1109/TIP.2013.2263809, 2014.

[15]. Zhang L., Zhang J., *A New Saliency-Driven Fusion Method Based on Complex Wavelet Transform for Remote Sensing Images*,

in IEEE Geoscience and Remote Sensing Letters, vol. 14, no. 12, p. 2433-2437, doi: 10.1109/LGRS.2017.2768070, 2017.

[16]. Jiang X., Mojon D. S., *Adaptive local thresholding by verification-based multithreshold probing with application to vessel detection in retinal images*, IEEE Transactions on Pattern Analysis and Machine Intelligence, 25 (1), p. 131-137, https://doi.org/10.1109/TPAMI.2003.1159954, 2003.

[17]. ***, *DRIVE: Digital Retinal Images for Vessel Extraction* (Image Sciences Institute, University Medical Center Utrecht), http://www.isi.uu.nl/Research/Databases/DRIVE/, 2004.

[18]. He K., Sun J., Tang X., *Guided image filtering*, IEEE Transactions on Pattern Analysis and Machine Intelligence, 35(6), p. 1397-1409, https://doi.org/10.1109/TPAMI.2012.213, 2013.

[19]. He K., Sun J., Tang X., *Guided image filtering*, IEEE Trans Pattern Anal Mach Intell, 35(6), p. 1397-409, doi: 10.1109/TPAMI.2012.213, PMID: 23599054, 2013.

[20]. Kou F., *et al.*, *Gradient Domain Guided Image Filtering*, IEEE Trans Image Process, 24 (11), p. 4528-39, doi: 10.1109/TIP.2015.2468183, 2015.

[21]. Mallat S., *A theory for multiresolution signal decomposition: The wavelet representation*, IEEE Transactions on Pattern Analysis and Machine Intelligence, 11 (7), p. 674-693, https://doi.org/10.1109/34.192463, 1989.

[22]. Donoho D. L., *De-noising by soft-thresholding*, IEEE Transactions on Information Theory, 41 (3), p. 613-627, https://doi.org/10.1109/18.382009, 1995.

[23]. Li S., Kang X., Hu J., *Image fusion with guided filtering*, IEEE Transactions on Image Processing, 22 (7), p. 2864-2875, https://doi.org/10.1109/TIP.2013.2244222, 2013.

[24]. Burt P. J., Adelson E. H., *The Laplacian pyramid as a compact image code*, IEEE Transactions on Communications, 31 (4), p. 532-540, https://doi.org/10.1109/TCOM.1983.1095851, 1983.

[25]. Shao Z., Cai J., *Remote Sensing Image Fusion with Deep Convolutional Neural Network*, IEEE Journal of Selected Topics in Applied Earth Observations and Remote Sensing, vol. 11, no. 5, p. 1656-1669, doi: 10.1109/JSTARS.2018.2805923, 2018.

[26]. Moraru L., *et al.*, *Retinal vessel enhancement based on the Gaussian function and image fusion*, AIP Conf. Proc., 1796 (1), 040007, https://doi.org/10.1063/1.4972385, 2017.

[27]. Li R., *et al.*, *A survey of multi-source image fusion*, Multimed Tools Appl, 83, p. 18573-18605, https://doi.org/10.1007/s11042-023-16071-9, 2024.